Rapid Communications

Two mechanisms of momentum transfer in granular flows

Matthew Macaulay* and Pierre Rognon

Particles and Grains Laboratory, School of Civil Engineering, University of Sydney, Sydney, New South Wales 2006, Australia

(Received 7 November 2019; accepted 3 April 2020; published 4 May 2020)

This Rapid Communication highlights the physical processes at the origin of the constitutive law of dense granular flows. In simulated plane shear flows, we present a micro-mechanical expression for the phenomenological friction law $\mu(\mathcal{I})$. The expression highlights two distinct pathways for momentum transport—through either balanced contact forces or grain micro-acceleration. We show that these two rate-dependent processes control and explain the friction law. This understanding may help advance rheological models for granular materials and other soft materials such as emulsions and suspensions.

DOI: 10.1103/PhysRevE.101.050901

Granular materials flow like no other liquid, and their flowing behavior has been perplexing scientists for decades [1–8]. A major understanding breakthrough was the discovery of a continuum constitutive law named $\mu(\mathcal{I})$ [6,9,10]. It relates the shear $\tau = (\sigma_{xy} + \sigma_{yx})/2$ and normal $P = (\sigma_{xx} + \sigma_{yy})/2$ stresses by a simple law reminiscent of Coulomb friction $\tau = \mu P$. The complexity of granular flows is embedded in the effective coefficient of friction μ, which exhibits multiple dependencies with the rate of shear $\dot{\gamma}$, the normal stress, the grain size d, and the grain density ρ. A dimensional analysis simplified these multiple dependencies to a single dependence with one dimensionless number, named the inertial number $\mathcal{I}$ [11]. Analysis of various flows showed that the friction coefficient increases from a minimum value μ_0 in the quasistatic regime ($\mathcal{I} \to 0$), up to a plateau at μ_2 in the collisional regime ($\mathcal{I} \gtrsim 1$) [9,10]. The following mathematical expression was proposed to capture this:

$$\mu(\mathcal{I}) \approx \mu_0 + \frac{\mu_2 - \mu_0}{\mathcal{I}_0/\mathcal{I} + 1}, \quad \mathcal{I} = t_i \|\dot{\gamma}\|, \quad t_i = d\sqrt{\frac{\rho}{P}}. \quad (1)$$

The parameters μ_0, μ_2, and $\mathcal{I}_0$ depend on the physical and geometrical properties of the grains. The inertial time t_i represents a characteristic timescale associated with inertial grain motion driven by a normal stress P. This friction law has a proven ability to predict flows in a variety of configurations [12]. However, it is phenomenological, and its physical origin remains unclear [1,11,13–16].

To identify the physical processes governing this constitutive law, we simulated a series of plane shear flows using a discrete element method. In this configuration, an assembly of grains is sheared at a constant shear rate $\dot{\gamma}$ and normal stress P, which together correspond to a single value of $\mathcal{I}$ [see inset of Fig. 1(a)]. Plane shear has the advantage of producing steady and homogeneous flows, where the stresses and strain rate are statistically invariant in time and space. We performed a number of such steady shear flows with different values of $\mathcal{I}$, from which we simultaneously measured the friction law $\mu(\mathcal{I})$ and microscopic quantities characterising contact forces and grain kinematics. The numerical technique and parameter values used for these simulations are detailed in the Supplemental Materials [17]. The results of the simulations support the following discussion.

Figure 1(a) shows that the frictional constitutive law measured in our simulations matches (1). To measure the coefficient of friction μ in any given test, we calculated the Cauchy stress tensor from the contact forces as $\sigma_{ij} = \mathrm{sym}(n_c \langle F_i l_j \rangle)$, where F_i and l_j are the ith and jth component of a contact force and branch vector, respectively, and $\mathrm{sym}(A) = (A + A^T)/2$ is the symmetric part of a tensor A. n_c is the density of contacts (i.e., the number of contacts per unit volume), and $\langle F_i l_j \rangle$ is the spatial and temporal average over all the contacts of their moment tensor. The $\langle \cdot \rangle$ operator is the average operator defined as $\frac{1}{N_t}\frac{1}{N_c}\sum_{t=0}^{N_t}\sum_{c=0}^{N_C} \cdot$. In this definition, each interaction between two grains yields two "contacts" with opposing forces, and with branch vectors connecting the center of each grain to the point of contact. This expression for the Cauchy stress σ_{ij} readily links continuum stress to micro-mechanics. It was, for instance, previously used to establish a link between the the friction coefficient and the contact anisotropy, a purely geometric feature of the flow [16]. In the following, we propose an alternative expansion of this expression that highlights the micro-mechanical dynamical processes underpinning $\mu(\mathcal{I})$.

First, we observed in all our tests that $\langle F_i l_j \rangle$ was symmetrical and that both normal stresses σ_{xx} and σ_{yy} were nearly equal. This means that the shear stress is given by either $\tau \approx n_c \langle F_x l_y \rangle$ or $\tau \approx n_c \langle F_y l_x \rangle$.

Second, we expanded the expectation of the contact moment as $\langle F_y l_x \rangle = \langle F_y \rangle \langle l_x \rangle + \delta F_y \delta l_x C$, where $\delta F_y^2 = \langle F_y^2 \rangle - \langle F_y \rangle^2$ is the contact force variance, $\delta l_x^2 = \langle l_x^2 \rangle - \langle l_x \rangle^2$ is the contact length variance, and C is their correlation. Hereafter, δF_y and δl_x are referred to as the contact force and length fluctuations, respectively. By definition, C is the Person correlation coefficient between the sets F_y and l_x and was computed separately. It represents the product of the vertical component of the contact forces and the horizontal component

*matthew.macaulay@sydney.edu.au; https://sydney.edu.au/engineering/people/matt.macaulay.680.php

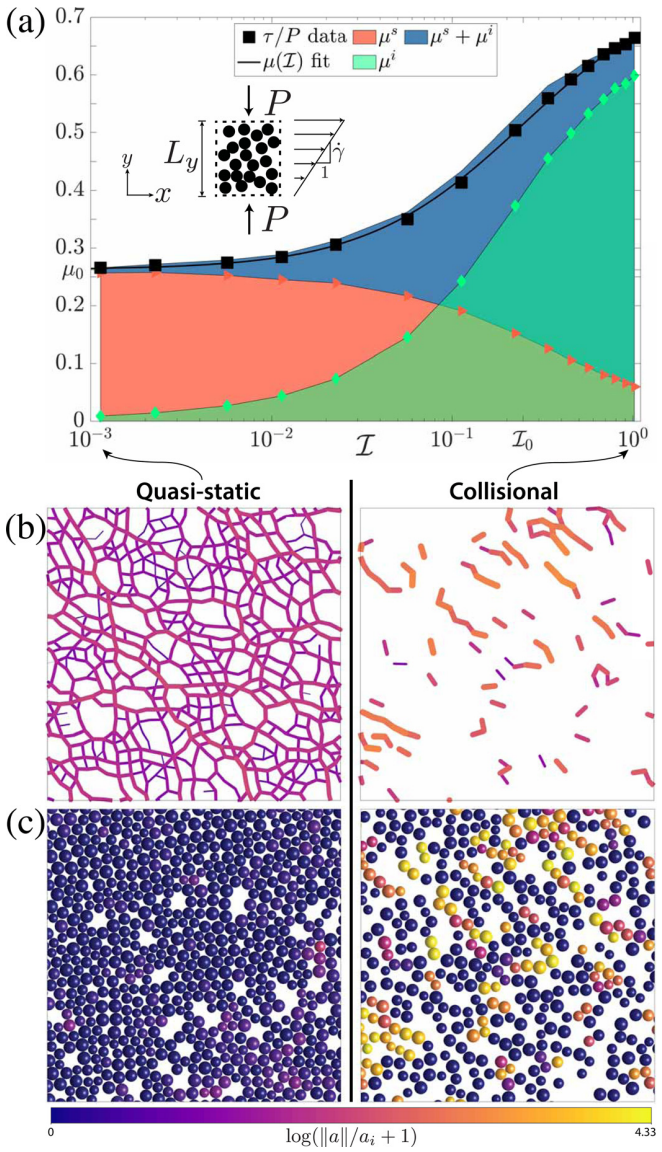

FIG. 1. *Granular friction law decomposition.* (a) Friction coefficient $\mu = \tau/P$ measured in simulated plane shear flows (■) fitted by the empirical friction law (1) (black line: best fit obtained using $\mu_0 = 0.26$, $\mu_2 = 0.88$, and $\mathcal{I}_0 = 0.29$), along with its decomposition into static μ^s and inertial μ^i parts (see text). Inset: Illustration of the plane shear configuration showing a linear velocity profile (arrows) and the periodic domain (dashed lines). (b, c) Snapshots of the contact force network and grain accelerations taken from flows in the quasistatic regime ($\mathcal{I} = 0.001$, left) and collisional regime ($\mathcal{I} = 1.0$, right). These show the rise in grain micro-acceleration and weakening of the contact force network at high inertial number, which control μ^s and μ^i, respectively (corresponding movies available online [17]). Segments in (b) connect the centers of two contacting grains, with linewidths proportional to $\log(1 + \|F\|/Pd^2)$ where $\|F\|$ is the norm of the contact force. Grains in (c) are colored according to the norm of their acceleration $\|a\|$.

of their branch vectors (this quantity differs from the correlation between force norm and contact orientation, as used in Ref. [16]). This set includes all contacts c in the flow detected at every recorded time t:

$$C := \frac{1}{N_t}\frac{1}{N_c}\frac{1}{\delta F_y \delta l_x}\sum_{t=0}^{N_t}\sum_{c=0}^{N_C}(F_y^c(t) - \langle F_y\rangle)(l_x^c(t) - \langle l_x\rangle). \quad (2)$$

Third, we observed that the average $\langle F_y\rangle$ and $\langle l_x\rangle$ are both null, which is consistent with the principle of opposing action-reaction forces at each contact. A pair of interacting grains involves two opposite forces and nearly opposite branch vectors (branch vectors would be perfectly opposite with monodisperse grains). Thus, the correlation C becomes

$$C = \frac{1}{\delta F_y \delta l_x}\langle F_y l_x\rangle. \quad (3)$$

Last, we measured that the contact length fluctuation was proportional to the grain size and nearly independent of $\mathcal{I}$: $\delta l_x = \alpha_l d$ with $\alpha_l = 0.72$. This analysis yields the following expression for the coefficient of friction $\mu = \tau/P$:

$$\mu(\mathcal{I}) = \beta\frac{\delta F_y}{Pd^2}, \quad \beta = \alpha_l n_c d^3 C, \quad (4)$$

as a product of the normalized force fluctuation $\delta F_y/Pd^2$ and a dimensionless number β measuring the density and the anisotropy of the contact force network. Figures 2 and 3 show that both these quantities vary with the inertial number: β decreases while δF_y increases linearly when $\mathcal{I}$ is increased.

The next argument is both pivotal and intuitive: that contact forces acting on a grain drive its micro-acceleration. While there is no net acceleration in the steady flows under consideration, individual grains can and do temporarily accelerate. To quantify these micro-accelerations, we have measured the quantity $\delta a^2 = \langle a^2\rangle - \langle a\rangle^2$, where a is the norm of the acceleration of a grain at a given time and $\langle\cdot\rangle$ is a temporal average over all the grains. δa is referred to as the acceleration fluctuation. When normalized by a characteristic inertial acceleration $a_i := d/t_i^2$, Fig. 2 (inset) shows that the acceleration fluctuation is proportional to the inertial number:

$$\mathcal{A} := \delta a/a_i \propto \mathcal{I}. \quad (5)$$

We call the dimensionless number $\mathcal{A}$ *micro-acceleration*. This highlights the following key relation between force and acceleration fluctuations:

$$\frac{\delta F_y}{Pd^2} \approx f_0 + \mathcal{A}(\mathcal{I}). \quad (6)$$

Our data indicate a value of $f_0 = 1.1$, close to unity [Fig. 2(a)]. The rationale for this linear increase is illustrated in Fig. 2(b): contact forces acting on a grain are only partially balanced. They comprise a balanced part that induces static stresses but no acceleration, $\delta F_y^b \approx Pd^2$, and an unbalanced part that drives grain micro-acceleration, $\delta F_y^u \propto m\delta a$, which yields $\delta F_y^u/Pd^2 \propto \mathcal{A}$. We further observed that both components δF_x^u and δF_y^u of the force fluctuations are nearly equal.

Combining Eqs. (4) and (6) enables us to express the friction law in terms of micro-quantities related to the contact network and the grain micro-acceleration:

$$\mu(\mathcal{I}) \approx \beta(\mathcal{I})[f_0 + \mathcal{A}(\mathcal{I})]. \quad (7)$$

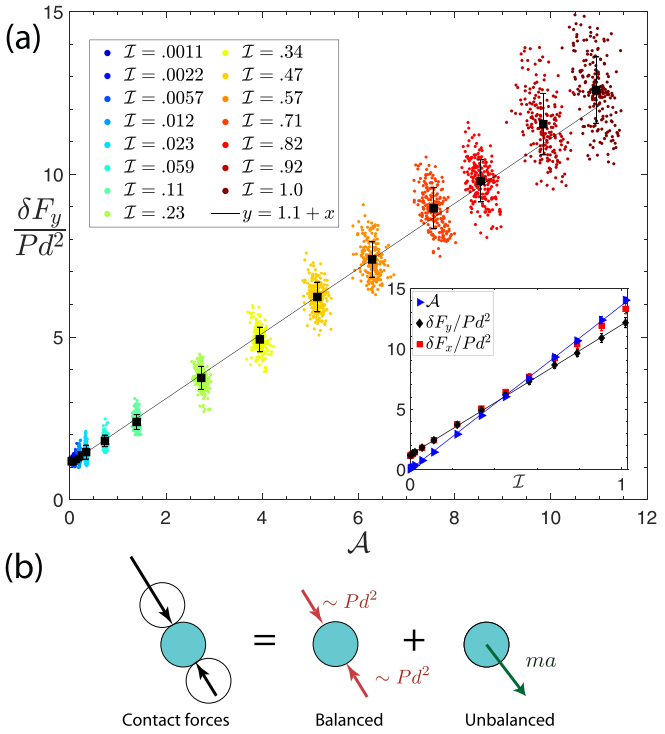

FIG. 2. *Rise of grain micro-accelerations driven by force fluctuations.* (a) The fluctuations in force increase linearly with the fluctuations in grain acceleration. Main panel: Each point represents the spatial average of one snapshot in time. Black square markers show their temporal average. The line shows the linear fit of Eq. (6) with $f_0 = 1.1$. Inset: Force and acceleration fluctuations both follow a linear dependence on the inertial number; markers show the measured force and acceleration fluctuations, and lines the best fits: $\mathcal{A} = 11\mathcal{I}$ and $\delta F_x/Pd^2 \approx \delta F_y/Pd^2 = 1.1 + 11\mathcal{I}$. (b) Illustration of two contact forces on a grain decomposing into a balanced part and an unbalanced part driving micro-acceleration.

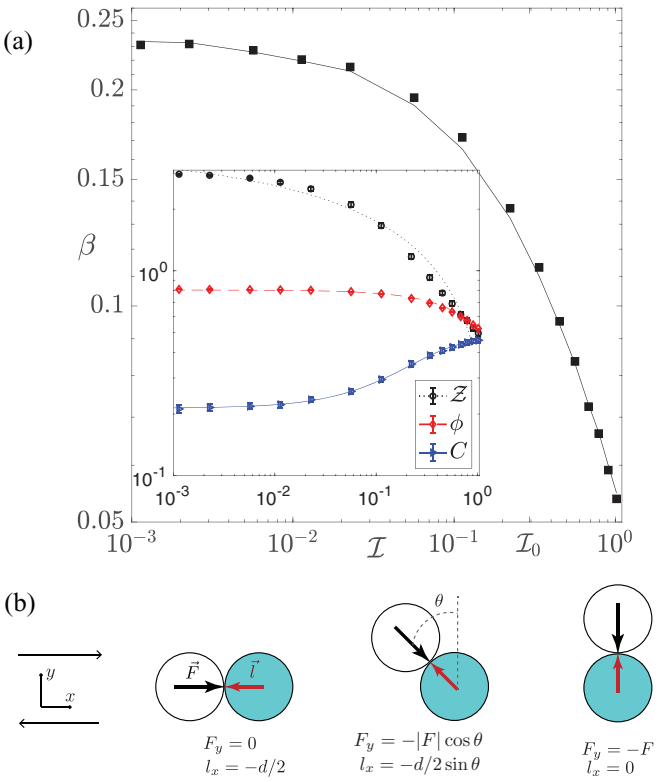

FIG. 3. *Contact network weakening.* (a) The contact network variable $\beta = \alpha_l n_c d^3 C$ decreases with increasing inertial number; the solid line represents the function $\beta = \mu/(f_0 + \mathcal{A})$ with no fit parameters. Inset shows that this decrease is driven by shear-induced dilation (reduced ϕ), which yields a decrease in coordination number $\mathcal{Z}$ as the inertial number is increased. The coordination number is the average number of contacts per grain, so that $n_c \propto \phi\mathcal{Z}$. Markers show the spatiotemporal average measured from our simulations. Lines represent the following best fits: $\mathcal{Z} = 4.0$–$3.7\mathcal{I}^{0.21}$, $\phi = 0.81$–$0.29\mathcal{I}$, and $C = 0.46$–$0.25\exp(-\mathcal{I}/0.29)$. (b) Illustration of contact orientations leading to different contributions towards C. Neglecting tangential contact forces, contacts in the shear direction and transverse to the shear direction do not contribute to C, since the product $F_y l_x = 0$. Contacts aligned with the principal stress direction ($\theta = \pi/4$) contribute the most (see text).

Accordingly, we propose to decompose the friction coefficient as a sum of two components:

$$\mu = \mu^s + \mu^i. \tag{8}$$

where $\mu^s(\mathcal{I}) = \beta(\mathcal{I})f_0$ is a static component supported by balanced contact forces, whereas $\mu^i(\mathcal{I}) = \beta(\mathcal{I})\mathcal{A}(\mathcal{I})$ is an inertial component arising from unbalanced forces.

Figure 1 confirms that this decomposition matches the continuum friction law. It also shows the variations of the components $\mu^s(\mathcal{I})$ and $\mu^i(\mathcal{I})$, which highlight the processes governing $\mu(\mathcal{I})$. In the quasistatic regime ($\mathcal{I} \to 0$), the inertial component is small, and the friction coefficient is predominantly controlled by the static component: $\mu(\mathcal{I} \to 0) \approx \mu^s(\mathcal{I}) = \beta(\mathcal{I})f_0$. As the inertial number increases, two processes simultaneously occur: the static component decreases while the inertial component grows. As a result, the friction coefficient is predominantly controlled by the inertial component in the collisional regime: $\mu(\mathcal{I} \gg \mathcal{I}_0) \approx \mu^i(\mathcal{I})$.

The decrease in static component is directly driven by $\beta(\mathcal{I})$, which itself is the product of the contact density and the correlation C. Figure 3 indicates that the decrease in $\beta(\mathcal{I})$ is caused by a decrease in contact density. This results from a dilatancy effect which leads to a decrease in solids fraction and coordination number; this implies fewer grains per unit volume and fewer contacts per grain. The snapshots of contact force networks shown in Fig. 1(b) further confirm these processes. In contrast, the correlation $C(\mathcal{I})$ appears to increase from about 0.2 to 0.4 when the inertial number is increased from 10^{-3} to 0.1, which hinders the decay in $\beta(\mathcal{I})$. This means that, while there are fewer contacts as $\mathcal{I}$ increases, each contact contributes more towards β.

In the following, we discuss the physical meaning of the correlation quantity C. The correlation can be expressed in terms of contact force $||F||$, branch vectors norm $||l||$, and their orientation θ:

$$C = \frac{1}{\delta F_y \delta l_x}\langle ||F||||l|| \cos\theta \sin\theta \rangle. \tag{9}$$

This means that the orientation of individual contacts influences their contribution to C. Horizontal ($\theta = \pi/2$) and

vertical ($\theta = 0$) contacts do not contribute to C. In contrast, the contact orientation that maximizes their contribution to C is $\pi/4$ from the flow direction. This orientation coincides with the orientation of the major principal stress in these shear flows, as we observed that the two normal stresses are equal. Figure 3(b) illustrates how this increase in C results from an increase in contact anisotropy, with the remaining contacts being more aligned with the major principal stress direction. We therefore interpret the increase is $C(\mathcal{I})$ to result from an alignment of contacts along the major principal stress. Such a shear-induced anisotropy was directly measured in Ref. [16].

The increase in inertial component $\mu^i(\mathcal{I}) = \beta\mathcal{A}$ is driven by the rise in grain micro-acceleration. Snapshots in Fig. 1(b) indicate that grain micro-accelerations rarely exceed the inertial acceleration a_i in the quasistatic regime, while they often are a few orders of magnitude higher in the collisional regime. However, the effect of this increase on μ^i is hindered by the decrease in the contact parameter $\beta(\mathcal{I})$.

The decomposition of the friction law into static and inertial components highlights a new understanding of the origin of the viscous behavior of granular materials. Granular dynamic viscosity is defined as $\eta = \mu P/|\dot{\gamma}|$ [9]; accordingly, a measure of granular kinematic viscosity is $\nu = \eta/\rho = (\mu^s + \mu^i)d^2|\dot{\gamma}|/\mathcal{I}^2$, which corresponds to a diffusivity of momentum. This indicates that momentum transport occurs by two distinct processes: either via a network of balanced contact forces that do not involve grain micro-acceleration, or via grain micro-accelerations themselves. We propose to decompose the granular viscosity ν into two components reflecting these processes:

$$\nu = \nu^s + \nu^i, \tag{10}$$

$$\nu^s = \frac{\beta(\mathcal{I})f_0}{\mathcal{I}^2}d^2|\dot{\gamma}|, \tag{11}$$

$$\nu^i = \frac{\beta(\mathcal{I})\mathcal{A}(\mathcal{I})}{\mathcal{I}^2}d^2|\dot{\gamma}|. \tag{12}$$

These viscosities correspond to momentum diffusivities. Their dimension is meters squared per unit time. Accordingly, they involve a characteristic length ℓ and timescale T, which both may depend on $\mathcal{I}$ such as $\nu^{s,i} \propto (\ell^{s,i})^2/T^{s,i}$. Our results indicates that the *static* and *inertial* viscosities have a different scaling with $\mathcal{I}$: $\nu^i(\mathcal{I}) \propto \mathcal{I}\nu^s(\mathcal{I})$, implying that they involve different characteristic lengths and/or different characteristic times. In the quasistatic regime ($\mathcal{I} \to 0$), the diffusivity length scales may be inferred by considering that $\beta(\mathcal{I}) \approx \mu_0$ and assuming that the characteristic timescale is the shear time $\dot{\gamma}^{-1}$. This leads to $\ell^s \propto d/\mathcal{I}$ and $\ell^i \propto d/\mathcal{I}^{.5}$. However, the assumption $T = \dot{\gamma}^{-1}$ is to be validated. For instance, it was shown that the characteristic time for mass diffusivity in dense granular flows involves the inertial number and is given by $I^{.5}\dot{\gamma}^{-1}$ [18,19]. Determining the characteristic time for momentum diffusion remains an open question.

The findings in this paper provide a basis to investigate how internal dynamics affect granular rheology in more complex flows. In inhomogeneous flows, the strain response may also depend on the spatial gradient of stress, rather than just the stress itself, and is termed a nonlocal flow [20–24]. For example, force fluctuations in a flow may propagate ("self-heat") into nonflowing regions and overcome the yield stress. Our decomposition suggests that nonlocality could arise from either the static or the inertial mode of momentum transport, or both. Comparing direct measurements of $\mu^i(\mathcal{I})$ and $\mu^s(\mathcal{I})$ in nonlocal flows against the local measurements presented here would enable one to directly identify which of these two modes of momentum transport is nonlocal.

Finally, our results and analysis are likely to be applicable to a wider class of materials comprising discrete "units" such as foams, emulsions, and dense suspensions [25–29]. We expect that the presence of interstitial water could require introducing a viscous time in place of the inertial time, and that the force-acceleration fluctuation relation we found for inertial grains might become a force-velocity fluctuation relation accounting for viscous interactions. In spite of these differences, we expect the two modes of momentum transport to be general features of these materials.

[1] R. Delannay, A. Valance, A. Mangeney, O. Roche, and P. Richard, J. Phys. D **50**, 053001 (2017).
[2] Y. Forterre and O. Pouliquen, C. R. Phys. **19**, 271 (2018).
[3] P. Jop, C. R. Phys. **16**, 62 (2015).
[4] Y. Forterre and O. Pouliquen, Annu. Rev. Fluid Mech. **40**, 1 (2008).
[5] F. Radjai and S. Roux, Phys. Rev. Lett. **89**, 064302 (2002).
[6] G. MiDi, Eur. Phys. J. E **14**, 341 (2004).
[7] J. Gaume, G. Chambon, and M. Naaim, Phys. Rev. E **84**, 051304 (2011).
[8] R. C. Hurley and J. E. Andrade, Granular Matter **17**, 287 (2015).
[9] P. Jop, Y. Forterre, and O. Pouliquen, Nature (London) **441**, 727 (2006).
[10] P. Jop, Y. Forterre, and O. Pouliquen, J. Fluid Mech. **541**, 167 (2005).
[11] F. da Cruz, S. Emam, M. Prochnow, J.-N. Roux, and F. Chevoir, Phys. Rev. E **72**, 021309 (2005).
[12] O. Pouliquen, C. Cassar, P. Jop, Y. Forterre, and M. Nicolas, J. Stat. Mech.: Theory Exp. (2006) P07020.
[13] T. Hatano and O. Kuwano, Pure Appl. Geophys. **170**, 3 (2013).
[14] L. E. Silbert, G. S. Grest, R. Brewster, and A. J. Levine, Phys. Rev. Lett. **99**, 068002 (2007).
[15] E. DeGiuli, J. N. McElwaine, and M. Wyart, Phys. Rev. E **94**, 012904 (2016).
[16] E. Azéma and F. Radjai, Phys. Rev. Lett. **112**, 078001 (2014).
[17] See Supplemental Material at http://link.aps.org/supplemental/10.1103/PhysRevE.101.050901 for the details of the plane shear flow simulations.
[18] P. Kharel and P. Rognon, Phys. Rev. Lett. **119**, 178001 (2017).
[19] P. Kharel and P. Rognon, EPL (Europhys. Lett.) **124**, 24002 (2018).
[20] K. Kamrin, Front. Phys. **7**, 116 (2019).
[21] K. Kamrin and G. Koval, Phys. Rev. Lett. **108**, 178301 (2012).

[22] M. Bouzid, M. Trulsson, P. Claudin, E. Clément, and B. Andreotti, Phys. Rev. Lett. **111**, 238301 (2013).
[23] T. Miller, P. Rognon, B. Metzger, and I. Einav, Phys. Rev. Lett. **111**, 058002 (2013).
[24] P. G. Rognon, T. Miller, B. Metzger, and I. Einav, J. Fluid Mech. **764**, 171 (2015).
[25] D. T. Chen, Q. Wen, P. A. Janmey, J. C. Crocker, and A. G. Yodh, Annu. Rev. Condens. Matter Phys. **1**, 301 (2010).
[26] C. Ancey, P. Coussot, and P. Evesque, J. Rheol. **43**, 1673 (1999).
[27] E. DeGiuli, G. Düring, E. Lerner, and M. Wyart, Phys. Rev. E **91**, 062206 (2015).
[28] J. Goyon, A. Colin, G. Ovarlez, A. Ajdari, and L. Bocquet, Nature (London) **454**, 84 (2008).
[29] V. V. Vasisht, S. K. Dutta, E. Del Gado, and D. L. Blair, Phys. Rev. Lett. **120**, 018001 (2018).